ELSEVIER

Polymer 43 (2002) 11–20

polymer

www.elsevier.com/locate/polymer

Plasma polymerized thiophene: molecular structure and electrical properties

M.S. Silverstein*, I. Visoly-Fisher[1]

Department of Materials Engineering, Technion — Israel Institute of Technology, Haifa 32000, Israel

Received 3 July 2001; received in revised form 12 August 2001; accepted 19 August 2001

Abstract

Polythiophene (PTh) is of interest for transistors, light emitting diodes and sensors. Plasma polymerization is a solvent-free, room temperature process that can be used to rapidly deposit thin polymer films onto a wide variety of substrates. This paper describes the synthesis of plasma polymerized thiophene (PPTh) and the dependence of molecular structure and properties on the polymerization conditions. Transparent plasma polymerized thiophene films, deposited at about 50 nm min^{-1}, had a density of about 1.75 g cc^{-1}, depending on the carrier gas used (if any) and on the plasma power. The molecular structure consisted of opened thiophene rings and included significant amounts of unsaturation, oxygen and nitrogen. When nitrogen was used as a carrier gas at a low power or when a high power was used (with no carrier gas), there was significantly more oxygen, nitrogen, and sulfur–oxygen bonds. When a high power was used, the films exhibited a higher polar component of surface tension and a higher internal stress. The undoped films exhibited non-linear current–voltage (IV) behavior typical of Schottky metal-semiconductor barriers with breakdown at reverse bias. Iodine doping yielded ohmic IV behavior, perhaps reflecting the formation of a conducting iodine percolation network.

Keywords: Plasma polymerization; Polythiophene; Thin films

1. Introduction

Intrinsically conductive polymers, polymers whose molecular structure provides a mechanism for the conduction of electricity, are being used in an increasing number of applications [1]. Conjugated polymers, such as polyacetylene, polypyrrole, polythiophene (PTh), polyaniline and their derivatives, become conductive when doped with a suitable oxidizing reagent. PTh is, both in its neutral and anion doped states, among the more environmentally stable and heat resistant of the intrinsically conductive polymers. PTh is of interest for both its electronic and optoelectronic properties, for such devices as transistors, light emitting diodes and sensors [2].

Grignard coupling or oxidative polymerization of thiophene (Th) yields an intractable polymer powder [3]. Two directions have been explored for the development of conducting PTh films. Electrochemical polymerization of thiophene can be used to synthesize an intractable PTh film on the anode. Electrochemical PTh films can be synthesized in the doped state by using suitable counter-ions such as BF_4^- or AsF_6^- [4]. However, in electrochemical polymerization, the yield is low and the polymers often do not have a well-defined structure. Oxidative or Grignard coupling polymerization of thiophene derivatives, such as 3-hexylthiophene, can yield well-defined conductive polymers that are soluble in organic solvents. Dopants commonly used for PTh's include I_2 and $FeCl_3$.

Plasma polymerization is a solvent-free, room temperature process that can be used to rapidly deposit thin polymer films onto a wide variety of substrates [5,6]. In plasma polymerization, a neutral 'monomer' gas or vapor in a low pressure reactor is subjected to an electric field. The monomer is fragmented into reactive species, which subsequently recombine, forming a polymer. The monomer can be a hydrocarbon, fluorocarbon, organosilicon or organometallic and need not necessarily include the functional groups typically associated with conventional polymerization techniques [5]. The molecular structure and properties of the plasma polymer depend on the monomer, gas phase composition, monomer flow rate, reactor pressure and plasma power. The advantages of plasma polymerization include: the environmental friendliness of the solvent-free process; the deposition of ultra-thin films with thickness directly proportional to deposition time; the deposition of pinhole-free

* Corresponding author. Tel.: +972-4-829-4582; fax: +972-4-832-1978.
E-mail address: michaels@tx.technion.ac.il (M.S. Silverstein).
[1] Present address: Department of Materials and Interfaces, Weizmann Institute of Science, Rehovot 76100.

0032-3861/02/$ - see front matter
PII: S0032-3861(01)00582-1

Table 1
Plasma polymerization conditions and plasma polymer properties

Plasma polymer	PPTh(10)	PPTh(10,Ar)	PPTh(10,N_2)	PPTh(150)
Gas added	None	Ar	N_2	None
Power (W)	10	10	10	150
Pressure (Pa)	160	160	160	67
F_m(Th) (sccm)	7.5	7.5	7.5	8.2
W/F_m(Th) (MJ kg^{-1})	21	21	21	292
F_m(gas) (sccm)	–	2	4	–
R_d (nm min^{-1})	47	40	60	35
ρ (g cc^{-1})	1.80	1.74	1.78	1.75

films without the dimensional changes associated with solvent evaporation; the deposition of highly adherent films with substrate activation in the plasma environment; the plethora of monomers available; and the simplicity of the reactor (standard microelectronics industry plasma deposition equipment). Previous investigations of plasma polymerized fluorocarbons [7–11], plasma polymerized hydrocarbons [12] and plasma polymerized organosilicons [13,14] have revealed that the synthesis conditions can be varied to yield significant changes in both molecular structure and properties.

Plasma polymerization has been used to synthesize semiconducting films using pyrrole and acrylonitrile derivatives [15–18]. This paper describes the synthesis of plasma polymerized thiophene (PPTh) using various polymerization conditions, the dependence of the PPTh molecular structure on the synthesis conditions. The relationships between the PPTh molecular structure and the physical, thermal, mechanical and electrical properties of PPTh films are investigated.

2. Experimental

2.1. Synthesis

The plasma polymerization was carried out in a commercial parallel-plate electrode radio frequency (13.56 MHz) plasma reactor (Jupiter III, March Instruments) that has been described in detail elsewhere [7]. The reactor could be evacuated to 2.5 Pa with a rotary vacuum pump (AC-2012, Alcatel) and the temperature of the anodized aluminum parallel-plate electrodes was maintained at 20°C with a circulating liquid cooler (RTE-100, Neslab). A flask of thiophene was attached to one of the reactor inlets. Plasma polymerizations were carried out with and without a carrier gas. The carrier gases used were argon and nitrogen. When there was no carrier gas, the vapor pressure of the thiophene yielded a sufficient flow into the low pressure reactor. The thiophene mass flow rate, F_m(Th), carrier gas mass flow rate, F_m(gas), pressures and powers used are listed in Table 1. This paper describes three thiophene plasma polymers from depositions at a plasma power of 10 W, a reactor pressure of 160 Pa and an F_m(Th) of 7.5 sccm as well as one thiophene plasma polymer from deposition at a plasma power of 150 W (PPTh(150)) at a significantly lower pressure and a higher F_m(Th). The thiophene plasma polymers deposited at 10 W include one without a carrier gas, one with argon and one with nitrogen: PPTh(10), PPTh(10,Ar) and PPTh(10,N_2), respectively. F_m(gas), calibrated separately, was always kept less than the F_m(Th) when no carrier gas was used.

The substrates ranged from glass slides (with or without an indium tin oxide (ITO) coating) to silicon wafers (with or without an aluminium coating) to KBr pellets. The polymerization procedure included cleaning the substrate in an argon plasma. The substrate was centered on the bottom electrode, the reactor was evacuated to 13 Pa, the substrate (except KBr) was cleaned with an argon plasma (100 W, 100 Pa, and 16.9 sccm) for 5 min before the reactor was again evacuated to 13 Pa prior to plasma polymerization. The desired F_m(Th), F_m(gas) (if applicable) and pressure were then attained and the plasma was ignited for a specific time. The molar flow rates and the reactor pressure were maintained constant throughout. After the plasma was extinguished, the thiophene and carrier gas (if applicable) feeds were closed, the reactor was evacuated to 13 Pa, and then the reactor was opened to the atmosphere.

2.2. Doping

The films were doped through exposure to I_2 vapor for about 25 min. The mass increased on doping and then decreased somewhat during storage. All the measurements on doped films took place after storage for the same time period. The mass of the samples indicated that the dopant was still present.

2.3. Characterization

The film thickness was measured using a profilometer with an accuracy of 0.05 μm (α-Step100, Tencor). The deposition rate, R_d, was calculated both in terms of mass per time and in terms of thickness per time. The density was calculated by dividing the mass gain by the substrate area and film thickness.

The molecular structure was characterized using a combination of X-ray photoelectron spectroscopy (XPS) and Fourier transform infrared spectroscopy (FTIR). An Al K_α

source XPS was used (Kratos, Axis-HS). Both low-resolution survey spectra and high-resolution core level spectra were taken for carbon, sulfur, nitrogen and oxygen. The high-resolution peak areas were evaluated following Shirley background subtraction [19]. The plasma polymers were deposited on KBr pellets for FTIR characterization (Nicolet, Impact 400).

The UV absorbance was measured using a UV–visible spectrometer (ATI/Unicam, UV2) in the 180–900 nm range. The absorbance at wavelength λ, A(λ), is the natural logarithm of the ratio of incident intensity to transmitted intensity. The substrates used for the electrical measurements were either ITO on glass or 1.2 μm of aluminum on silicon. One corner of the substrate was covered such that it would not be coated during plasma polymerization. Following the deposition of the films, a number of 30 nm thick circular gold contacts with a 1 mm diameter were evaporated onto the films via a mask. The IV characteristics were measured using a two probe configuration between the gold contact and between the corner of the substrate left uncoated. The resistance of the contacts is assumed to be negligible compared to the resistance of the film. The current (I) was measured as a function of the applied voltage (V) from −5 to +5 V using a voltage source and a pico-ammeter with an accuracy of 10^{-9} A (Keithley, 487). The conductivity, σ, was calculated using Eq. (1):

$$\sigma = \frac{Id_f}{VA_c} \tag{1}$$

where d_f is the film thickness and A_c is the contact area.

3. Results and discussion

3.1. Deposition rate

PPTh mass and thickness varied linearly with deposition time and the deposition rates, R_d, are listed in Table 1. R_d has been related to W/F_m(Th), the ratio of plasma power, W, to monomer mass flow rate [5,9]. W/F_m(Th), which expresses the plasma energy per mass monomer, is 21 MJ kg^{-1} for the polymerizations at 10 W. Transparent, yellowish PPTh(10) films were deposited at a relatively low deposition rate (47 nm min^{-1}, Table 1). In spite of the unusually high pressure used in these polymerizations (160 Pa), there was no powder formation in the area of the sample. Adding argon at a constant pressure reduces R_d from 47 to 40 nm min^{-1}. This reduction in R_d is attributed to the reduction in the partial pressure of the monomer, i.e. in the concentration of reactive species. In addition, Ar, with its high atomic mass, is commonly used for plasma cleaning through physical etching. The reduction in R_d also reflects etching from argon ion bombardment [8,12]. Adding nitrogen at a constant pressure, however, augments R_d to 60 nm min^{-1}. This increase in R_d can be attributed to the incorporation of nitrogen into the plasma polymer, as seen for other plasma polymerizations [8,12].

A significantly lower pressure (67 Pa instead of 160 Pa) and a slightly higher F_m(Th) were used to prevent powder formation for plasma polymerization at 150 W. The reduction in R_d to 35 nm min^{-1} reflects both the reduced concentration of reactive species (i.e. the reduced pressure) and the augmentation of etching at the higher power. Here, again, transparent, yellowish films were deposited with no sign of powder formation, in spite of the relatively high power (and W/F_m(Th)) that tends to enhance powder formation [5].

The densities, ρ, of the plasma polymers are listed in Table 1. The average density of the four plasma polymers is 1.77 g cc^{-1}. The density of the PPTh films is significantly higher than the 1.5 g cc^{-1} density of PTh [20]. A higher density in plasma polymerized hydrocarbons that can reflect an unsaturated structure has also been observed for plasma polymerized ethylene [12]. Given the experimental errors involved, the slight differences in density among the PPTh films do not seem significant. Despite the similarities in density, however, the molecular structures of the plasma polymers are quite different.

3.2. Molecular structure

The FTIR transmission spectrum for PPTh(10) in Fig. 1 not only contains bands that represent carbon–carbon and carbon–sulfur bonds but also contains prominent bands that can represent carbon–oxygen, sulfur–oxygen and carbon–nitrogen bonds. Bands (**a**) and (**j**) (3417 and 1042 cm^{-1}) represent hydroxyl groups; bands (**b**) and (**c**) (2957 and 2861 cm^{-1}) represent CH_3 and CH_2 groups; bands (**d**) and (**e**) (2209 and 2051 cm^{-1}) represent X=Y=Z where X, Y and Z can be a combination of C, S, O or N; bands (**f**) and (**g**) (1674 and 1625 cm^{-1}) represents X–C=O, carbonyl, carboxyl, amide and thiol ester; band (**h**) (1447 cm^{-1}) represents CH_2–S; the bands between (**i**) and (**j**) (1254 to

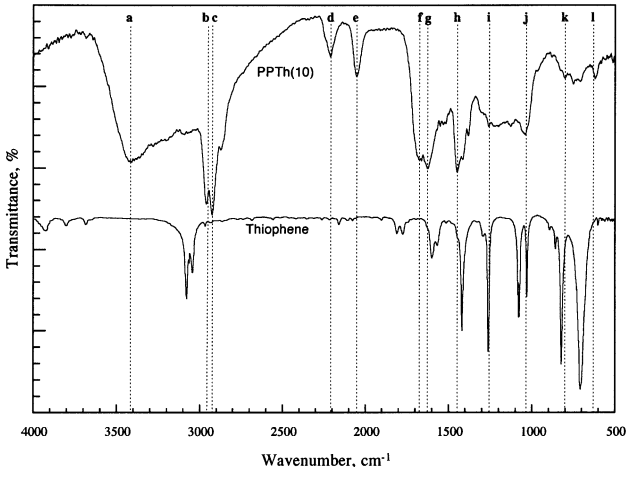

Fig. 1. FTIR spectra of thiophene and PPTh(10).

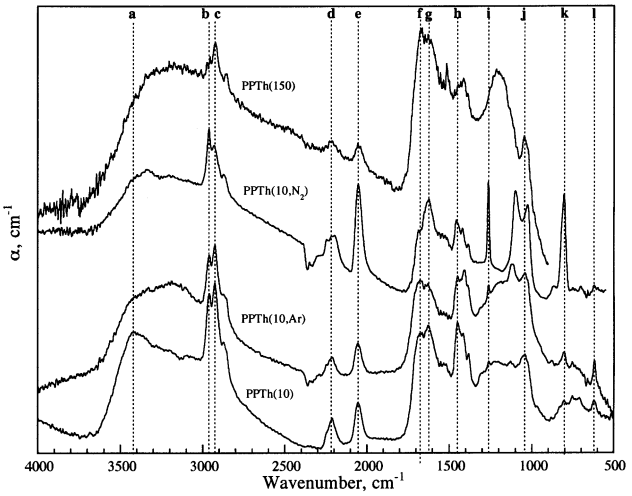

Fig. 2. FTIR spectra of the PPTh films.

1042 cm^{-1}) represent carbon–oxygen and sulfur–oxygen bonds; the bands between (**k**) and (**l**) (802 to 624 cm^{-1}) represent C=C bonded to non-alkyl [21].

Unlike the FTIR spectra for thiophene (Fig. 1) and conventional PTh [22], the FTIR spectrum for PPTh(10) indicates significant oxygen and nitrogen contents. The FTIR bands typical of the thiophene ring, seen in thiophene (1590 and 1400 cm^{-1}, Fig. 1) and conventional PTh (1490 and 1400 cm^{-1}), are not prominent in PPTh(10). The lack of these bands indicates that exposure to the plasma has opened the thiophene rings. The PPTh(10) FTIR bands are especially wide, reflecting that the molecular structure of a plasma polymer originates in the random assembly of molecular fragments.

The absorption spectra for the plasma polymerized films are seen in Fig. 2. In general, the spectra for the different plasma polymerized films are quite similar. Selected band heights, normalized by the height of the methylene band at 2957 cm^{-1}, are compared in Table 2. The normalized band heights for PPTh(10) and PPTh(10,Ar) are quite similar in most respects. The normalized band heights associated with oxygen at 1627 cm^{-1} for PPTh(150) is more than three times that for PPTh(10). This increase in normalized band height is also true for most of the other bands associated with either oxygen or nitrogen. These differences in the normalized band heights indicate that PPTh(150) has significantly larger oxygen and/or nitrogen contents than do PPTh(10) and PPTh(10,Ar).

The bands (**i**) and (**k**) (1254 and 802 cm^{-1}) are especially prominent for PPTh(10,N_2). These bands are typical of $Si–CH_3$ [21] and reflect contamination of the film by the silicone vacuum grease used to seal the glass fittings. The CH_3 in the silicone vacuum grease will also contribute to the height of band (**b**), the methylene band at 2957 cm^{-1}, used for the normalization in Table 2. Table 2 indicates that PPTh(10,N_2) has significantly more X=Y=Z groups and significantly more X–C=O groups. The normalizing peak is augmented by the presence of silicon grease and, therefore, the increase in X=Y=Z and X–C=O groups is even greater than it appears from the data in Table 2. Thus, the oxygen and nitrogen contents of PPTh(10,N2) and PPTh(150) are expected to be significantly greater than those of PPTh(10) and PPTh(10,Ar).

The elemental percentages from XPS, x_i (where i is an element), reveal that there are significant amounts of nitrogen and oxygen in all the plasma polymers (Table 3). Oxygen is often found in plasma polymers and is commonly attributed to the reaction of long-lived radicals with atmospheric oxygen [5]. Adding argon to the feed reduces the oxygen content, as seen for other plasma polymers [8,12]. Nitrogen is not generally incorporated into plasma polymers through atmospheric exposure [5]. The significant nitrogen content in PPTh(10), PPTh(10,Ar) and PPTh(150) is, therefore, unusual. There was no detectable leak in the vacuum system nor was there the telltale nitrogen pink in the plasma glow. The nitrogen in the plasma polymers might originate in residual air in the system at the relatively high base pressure used or in the reaction of atmospheric nitrogen with a specific long-lived radical produced in the sulfur-containing plasma. The 1.4% silicon in PPTh(10,N_2) is consistent with the silicone vacuum grease contaminant found using FTIR.

Thiophene has a carbon to sulfur ratio of 4 and conventional polythiophene exhibits similar x_C/x_S ratios [23]. PPTh(10) and PPTh(10,Ar) exhibit x_C/x_S ratios of about 6. This larger x_C/x_S ratio indicates that sulfur is preferentially included in the volatile products formed in the plasma and is evacuated by the vacuum. This preferential loss of sulfur is consistent with the lower energy of the S–C bond (272 kJ mol^{-1}) compared to the higher energy of the C–C

Table 2
Selected FTIR band heights normalized by the 2957 cm^{-1} band height

Band	**b**	**e**	**g**
Band (cm^{-1})	2957	2051	1627
Groups	CH_3, CH_2	X=Y=Z[a]	X–C=O[a]
PPTh(10)	1	0.41	1.15
PPTh(10,Ar)	1	0.45	1.20
PPTh(10,N2)	1	2.07	2.01
PPTh(150)	1	0.53	4.07

[a] X, Y and Z are a combination of C, S, O or N.

Table 3
x_i and x_C/x_S from XPS

	PPTh(10)	PPTh(10,Ar)	PPTh(10,N_2)	PPTh(150)
x_C (%)	70.9	72.3	58.0	54.0
x_S (%)	12.4	11.4	8.6	14.4
x_N (%)	8.7	10.3	14.6	11.1
x_O (%)	8.0	5.6	17.4	20.5
x_{Si} (%)	0	0.4	1.4	0
x_C/x_S	5.72	6.34	6.74	3.75

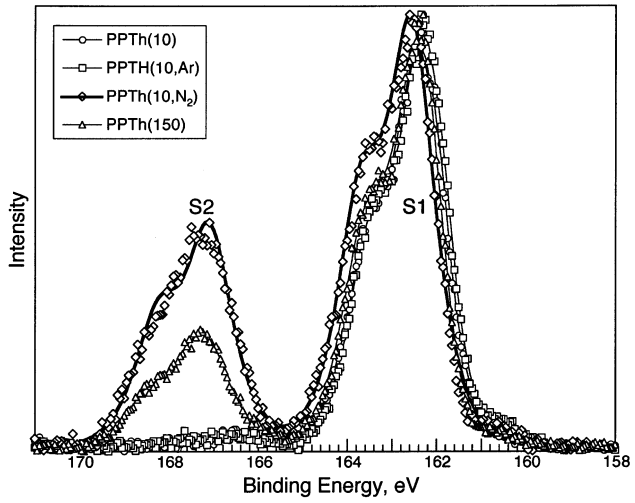

Fig. 3. S_{2p} spectra of the PPTh films.

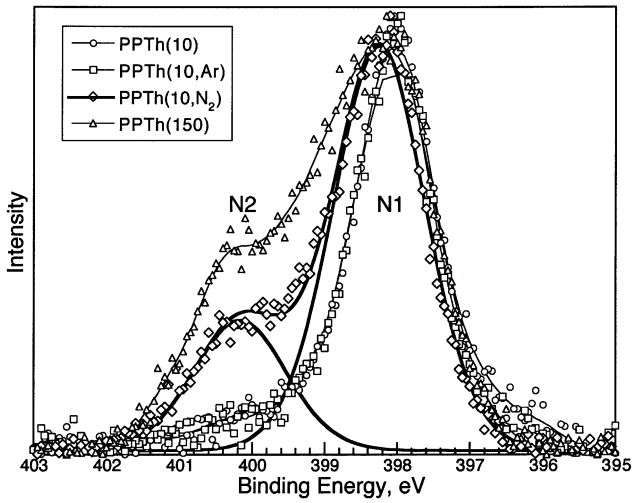

Fig. 4. N_{1s} spectra of the PPTh films.

and C–H bonds (348 and 415 kJ mol^{-1}, respectively) [24]. The x_C/x_S ratio is even higher in PPTh(10,N_2), indicating that nitrogen incorporation is favored over sulfur incorporation (the energy of the C–N bond is 306 kJ mol^{-1}). The significant increase in oxygen content on the introduction of nitrogen into the feed has been attributed to the formation of radicals in the nitrogen-containing plasma polymer that are more likely to react with atmospheric oxygen [8,12].

The x_C/x_S of 3.75 for PPTh(150) is similar to that of thiophene. This thiophene-like x_C/x_S, however, does not indicate that PPTh(150) has a thiophene-like structure. At 150 W, the processes of monomer fragmentation and plasma etching are more intense. The more intense destructive processes increase the carbon content of the volatile products, thus reducing the carbon content in the plasma polymer. The higher power would also produce a higher concentration of long-lived free radicals to react with the atmosphere, thus increasing the oxygen content.

The S_{2p} peaks are doublets. There is 1.2 eV between the peaks, and the higher binding energy peak has about half the intensity of the lower binding energy peak [25]. The films can be divided into two categories based on the S_{2p} peaks in Fig. 3. Both PPTh(10) and PPTh(10,Ar) exhibit one doublet peak (**S1**), at approximately 162.8 eV. **S1** is associated with sulfur that is bound to carbon and excludes additional bonds to oxygen [26]. Both PPTh(10,N_2) and PPTh(150) exhibit a second doublet peak (**S2**), at approximately 168.7 eV. **S2** is associated with sulfur that is bound to oxygen, but this does not exclude additional bonds to carbon [26]. The thick lines in Fig. 3 are the results of the curve fit for the PPTh(10,N_2) S_{2p} spectrum that divides the spectrum into **S1** and **S2** peaks as well as the sum of the **S1** and **S2** peaks that corresponds to the experimental data. The area fractions of **S1** and **S2** for PPTh(10,N_2) are 66 and 34%, respectively. Over one third of the sulfur in PPTh(10,N_2) has bonds to oxygen. Similarly, **S1** and **S2** constitute 78 and 22%, respectively, of the S_{2p} spectrum for PPTh(150). Multiplying these area fractions by the sulfur content from Table 3, divides the elemental composition of sulfur into two categories: sulfur with no oxygen bonds (**S1**) and sulfur with oxygen bonds (**S2**). The contributions of **S1** and **S2** to the elemental compositions are seen in Table 4. PPTh(10), PPTh(10,Ar) and PPTh(150) have elemental **S1** sulfur contents that lie between 11.3 and 12.4%. PPTh(10,N_2) has a lower elemental **S1** content, 5.6%, reflecting the decrease in sulfur content with the increase in nitrogen content. PPTh(10,N_2) and PPTh(150) have similar elemental **S2** sulfur contents of 2.9 and 3.2%, respectively.

The N_{1s} spectra in Fig. 4 can also be divided into the same two categories found for the S_{2p} spectra. Both PPTh(10) and PPTh(10,Ar) exhibit one main peak (**N1**) at

Table 4
x_{S1}, x_{S2}, x_{N1}, and x_{N2} from the S_{2p} and N_{1s} curve fits

Content (%)	BE (eV)	Group	PPTh(10)	PPTh(10,Ar)	PPTh(10,N_2)	PPTh(150)
x_{S1}	162.8[a]	S–C	12.4	11.4	5.6	11.3
x_{N1}	399.7	N–C	8.1	10.0	11.1	7.6
x_{S2}	168.7[a]	SO_y	0.0	0.0	2.9	3.2
x_{N2}	401.8	N^+	0.6	0.4	3.6	4.9

[a] $S_{2p1/2}$.

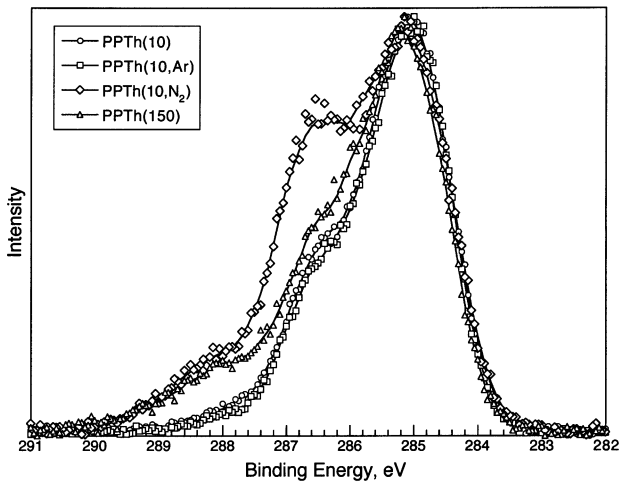

Fig. 5. C_{1s} spectra of the PPTh films.

approximately 399.7 and a small second peak (**N2**) at approximately 401.8 eV. Both PPTh(10,N_2) and PPTh(150), on the other hand, exhibit a significant **N2** peak. **N1** is typical of carbon–nitrogen bonds. **N2** is typical of ions such as C–NH_3^+. The thick lines in Fig. 4 are the results of the curve fit for the PPTh(10,N_2) N_{1s} spectrum that divides the spectrum into **N1** and **N2** peaks as well as the sum of the **N1** and **N2** peaks that corresponds to the experimental data. The area fractions of **N1** and **N2** for PPTh(10,N_2) are 75 and 25%, respectively. The **N2** area fraction for the PPTh(150) N_{1s} spectrum is much higher, at 39%, while the **N2** area fractions for the PPTh(10) and PPTh(10,Ar) N_{1s} spectra are much lower, at about 5%. Multiplying these area fractions by the nitrogen content from Table 3 divides the elemental composition of nitrogen into two categories: nitrogen with no ionic character (**N1**) and nitrogen with an ionic character (**N2**). The contributions of **N1** and **N2** to the elemental compositions are seen in Table 4. The films have elemental **N1** nitrogen contents that lie between 7.6 and 11.1%. PPTh(10,N_2) has the highest elemental nitrogen content and the highest elemental **N1** content. PPTh(10,N_2) and PPTh(150) have similar elemental **N2** contents of 3.6 and 4.9%, respectively. PPTh(10) and PPTh(10,Ar) have similar elemental **N2** contents of about 0.5%.

The C_{1s} spectra in Fig. 5 contain peaks that represent the presence of sulfur, oxygen, nitrogen and unsaturated groups. The C_{1s} peaks associated with nitrogen and oxygen are at higher binding energies than the C=C, C–C and C–S peaks, which are close together. The higher nitrogen and oxygen contents of PPTh(10,N_2) and PPTh(150) are immediately obvious from the significant shoulders at high binding energies.

Plasma polymers are random assemblies of molecular fragments and, therefore, the full width at half maximum (FWHM) of a specific C_{1s} peak is expected to be relatively large, about 2 eV [10]. The C_{1s} spectra for these films consist of peaks that are not only close together but also relatively broad, thus yielding significant overlapping. The spectra for all four films were curve fit using the same binding energy assignments (Table 5) and the same FWHM of 1.9 eV. The binding energy assignments for the almost completely overlapping C=C, C–C and C–S (284.7, 285.0 and 285.4 eV, respectively) were taken from the literature [25]. The peaks associated with carbon–oxygen bonds and with carbon–nitrogen bonds were assigned as a compromise between several groups with similar binding energies, the presence of obvious peaks in the data, and the desire to minimize the number of peaks used in the curve fit. The peak at 286.5 eV represents groups such as C–O, C–N and C=N; the peak at 288.0 eV represents groups such as C=O, N–C–O and N–C=O; and the peak at 289.0 eV represents O–C=O (Table 5).

The curve fit for the C_{1s} spectrum of PPTh(10,N_2) is seen in Fig. 6. There is abundant overlapping of the various peaks. The percentage that the individual C_{1s} curve fit peak areas contribute to the total C_{1s} spectrum area, A_j (where j represents the binding energy of the peak), are listed in Table 5. According to the curve fit, the films have C=C contents of about 19%, reflecting their origin in the unsaturated thiophene carbons. The sum of the C=C, C–C and C–S peak area percentages represents carbon with bonds to neither oxygen nor nitrogen. This sum is 72.0, 73.0, 54.7 and 63.4% for PPTh(10), PPTh(10,Ar), PPTh(10,N_2) and

Table 5
A_j, $x_{(O-C+N-C)}$, and x_{O-S} from the C_{1s} curve fits and $x_O + x_N$ from Table 3

		Content (%)			
	Group	PPTh(10)	PPTh(10,Ar)	PPTh(10,N_2)	PPTh(150)
$A_{284.7}$	C=C	25.6	16.6	19.6	16.0
$A_{285.0}$	C–C	21.1	35.5	17.6	15.3
$A_{285.4}$	C–S	25.3	21.2	17.5	32.1
$A_{286.5}$	C–N, C=N, C–O	24.7	24.6	35.7	25.4
$A_{288.0}$	C=O	3.3	2.1	7.9	8.3
$A_{289.0}$	O–C=O	0.0	0.0	1.7	2.9
$X_{(O-C+N-C)}$		19.9	19.3	27.3	21.3
$x_O + x_N$		16.7	15.9	32.0	31.6
x_{O-S}		–	–	4.7	10.3

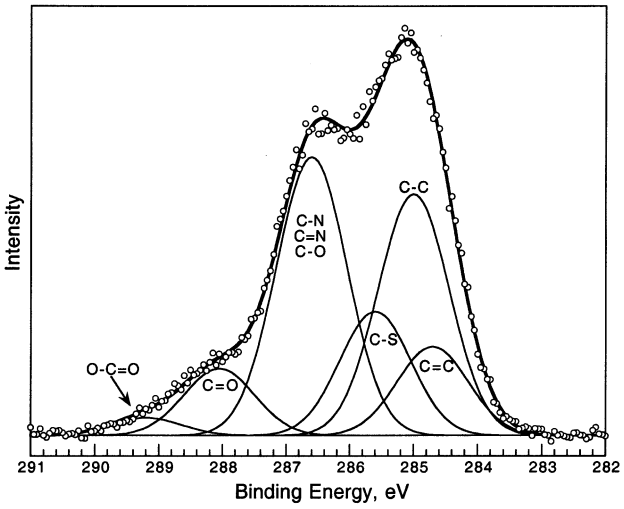

Fig. 6. Curve fit for the PPTh(10,N_2) C_{1s} spectrum.

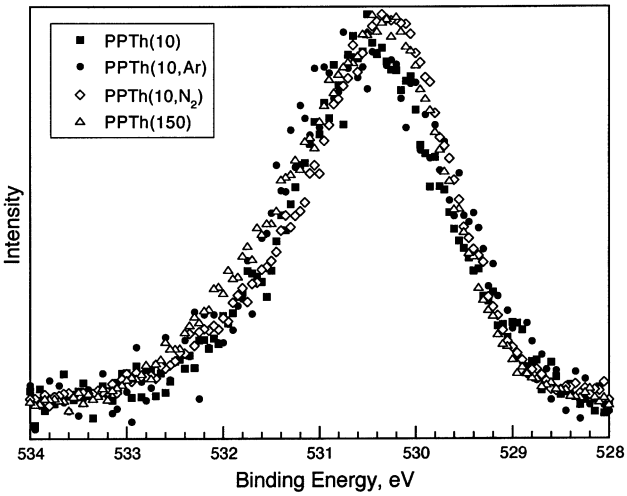

Fig. 7. O_{1s} spectra of the PPTh films.

PPTh(150), respectively. These sums reflect the relatively low oxygen and nitrogen contents of PPTh(10), PPTh(10,Ar) and the relatively high oxygen and nitrogen contents of PPTh(10,N_2) and PPTh(150) seen in the low resolution survey spectra. $A_{286.5}$ for PPTh(10,N_2), 35.7%, is significantly higher than that for the other films. The relatively high $A_{286.5}$ reflects the relatively high nitrogen content of PPTh(10,N_2), confirming that the peak at 286.5 eV reflects carbon–nitrogen bonds. Both PPTh(10,N_2) and PPTh(150) have significantly higher area fractions for the peaks at 288.0 and 289.0 eV, reflecting their significantly higher oxygen contents. The XPS results thus confirm the FTIR analyses.

The elemental percentage of oxygen bound to carbon plus nitrogen bound to carbon, $x_{(O-C+N-C)}$, can be calculated from the curve fit to the C_{1s} spectra in Table 5 and x_C from Table 3. It is not possible to separate the oxygen contributions from the nitrogen contributions since the C_{1s} peaks were chosen such that they represent the contributions from both carbon–oxygen and carbon–nitrogen bonds. Eq. (2) is used to calculate $x_{(O-C+N-C)}$ from the sum of the A_j's associated with oxygen and nitrogen ($j = 286.5$, 288.0 and 289.0 eV) and the results are listed in Table 5 along with $x_O + x_N$, the sum of the elemental percentages of oxygen and nitrogen from the low resolution spectra. PPTh(10) and PPTh(10,Ar) have similar $x_O + x_N$ (about 16.3%) and similar $x_{(O-C+N-C)}$ (about 19.6%). The 20% overestimate of the elemental percentage of oxygen plus nitrogen by $x_{(O-C+N-C)}$ is a result of the many assumptions made in the definition of a consistent C_{1s} curve fit. These results confirm the validity of the C_{1s} curve fit and support the use of $x_{(O-C+N-C)}$ to represent the elemental percentage of oxygen plus nitrogen bound to carbon.

$$x_{(O-C+N-C)} = (A_{286.5} + A_{288.0} + 2A_{289.0})^* x_C/100 \quad (2)$$

The comparison of $x_{(O-C+N-C)}$ and $x_O + x_N$ can be used to detect materials in which there is a significant amount of oxygen that is not bound to carbon. For both PPTh(10,N_2) and PPTh(150), Eq. (2) yields an $x_{(O-C+N-C)}$ that not only does not overestimate $x_O + x_N$, but is also smaller than $x_O + x_N$ (Table 5). For these two films, the difference between $x_O + x_N$ and $x_{(O-C+N-C)}$, x_{O-S}, represents the elemental percentage of oxygen bound to sulfur in SO_y (Table 5). This difference is quite significant in PPTh(150), where x_{O-S} is 10.3%, about half the x_O of 20.5%. The ratio of x_{O-S} to x_{S2} (sulfur bound to oxygen), about 1.6 for PPTh(10,N_2) and 3.2 for PPTh(150), yields reasonable estimates for y in SO_y. Thus, this detailed analysis of the C_{1s} spectra supports the conclusions drawn from the analysis of the S_{2p} spectra.

The O_{1s} spectra for all four films in Fig. 7 are quite similar, with maxima at 531.8 ± 0.1 eV. These spectra include contributions from C–O, C=O and O*–C=O at about 532.8, 532.3 and 533.6 eV, respectively, as well as bonds with sulfur, including SO_3^-, at about 531.7 eV [25,26]. Both PPTh(10,N_2) and PPTh(150) exhibit a more significant contribution from the lower binding energy peaks than PPTh(10) and PPTh(10,Ar), which also supports the conclusions regarding the presence of sulfur–oxygen bonds drawn from the analysis of the S_{2p} spectra.

The molecular structures of PPTh(10,N_2) and PPTh(150) are, thus, distinctly different from those of PPTh(10) and PPTh(10,Ar). PPTh(10,N_2)/PPTh(150) contain significant amounts of sulfur–oxygen bonds, perhaps including SO_3^-, and significant amounts of nitrogen, perhaps including NH_4^+, while PPTh(10)/PPTh(10,Ar) do not.

3.3. Optical and electrical properties

The optical absorption coefficient, α, is the absorption divided by the film thickness. The variation of α with photon energy for the various films is seen in Fig. 8. The

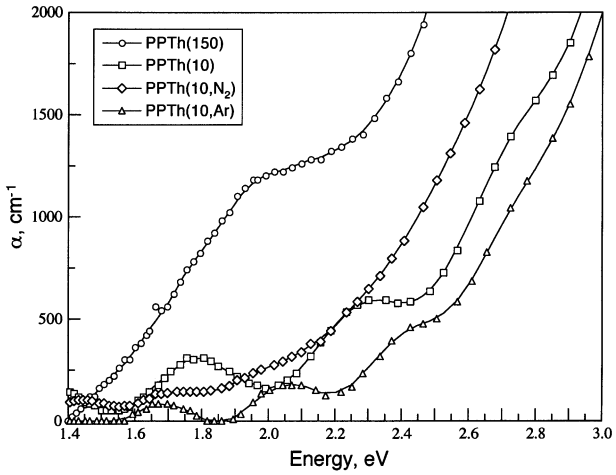

Fig. 8. Optical absorption of the PPTh films.

highest energy peaks or shoulders are similar to those seen for PTh band gap transitions. There is a rapid increase in absorption at approximately 2.6 eV (Fig. 8) that is typical of the high UV absorbance of polymeric materials.

The Mott equation, Eq. (3), describes the relationship between energy (E) and absorption coefficient (α) for amorphous semiconductors with a linear relationship between $(\alpha E)^{1/2}$ and E [27]. The Mott plot for PPTh(10) in Fig. 9, $(\alpha E)^{1/2}$ vs. E, and Eq. (3) were used to determine the band gap, E_g. The plasma polymer data at high energies in Fig. 9 exhibit the linear relationship described in Eq. (3). Extrapolating the line through the high-energy data to the x-axis yields an E_g of 2.3 eV. The deviation from linearity at low energies, the 'tail', is a feature typically found in Mott plots of amorphous semiconductors [27].

$$(\alpha E)^{1/2} = B(E - E_g) \tag{3}$$

where B is a constant.

The E_gs of the PPTh films derived from the Mott plots are around 2.2 eV (Table 6), typical of PTh [28]. Taking the band gap energies from the high-energy peak or from the distinct high-energy shoulders in Fig. 8 yields almost identical results. Only PPTh(10) exhibits a peak at E_g in Fig. 8. The other PPTh films exhibit shoulders at E_g, and the E_g shoulder for PPTh(10,N_2) was especially difficult to discern. For PPTh(150) there were no discernable transitions aside from the E_g. The shoulders at approximately 2.8 eV for PPTh(10) and PPTh(10,Ar) in Fig. 8 are typical of the $\pi-\pi^*$ transition seen in PTh [29]. The relatively small peaks at lower energies are also typical of PTh and represent energy states within the gap due to defects [30–32]. These can be charged defects that participate in conduction or structural defects that create localized energy states. The peaks at approximately 1.7 eV could indicate the presence of bipolarons, as are found in PTh. The other peaks are attributed to transitions reflecting the non-PTh structure of the films.

The variation of absorption coefficient with energy suggests that the plasma polymer films have dual natures: the properties of an insulator predominate, but there remain traces of properties that are typical of a semiconductor. One possible explanation for such a combination is the presence of intrinsically semiconducting 'islands' within an insulating matrix.

The optical properties reflect the molecular structures derived from FTIR and XPS: PPTh(10) and PPTh(10,Ar) have similar optical properties and molecular structures; PPTh(10,N_2) is somewhat different from the other two films deposited at 10 W; PPTh(150) is quite different from the other films. There is no sign of a $\pi-\pi^*$ shoulder for PPTh(10,N_2) or PPTh(150), indicating that their structures contain fewer ring-like molecules than do PPTh(10) and PPTh(10,Ar).

The insulating nature of PPTh(10) and PPTh(10,N_2) were such that the current–voltage (IV) characteristics could not be measured. The IV characteristics of PPTh(10,Ar) and PP(Th-150), in both the as-deposited and I_2 doped states, are seen in Fig. 10. The IV characteristics of the

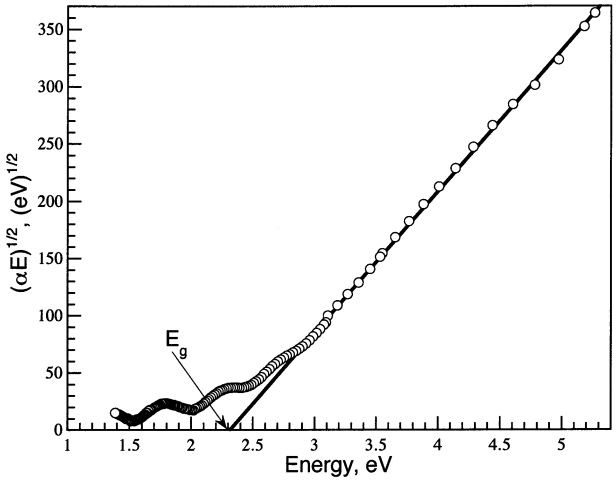

Fig. 9. Mott plot for PPTh(10).

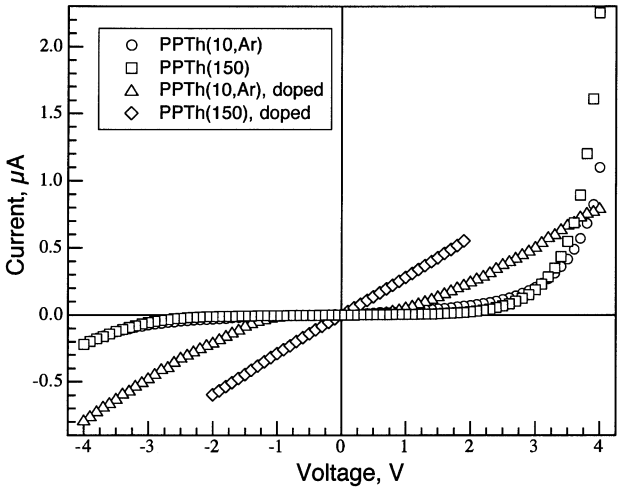

Fig. 10. IV characteristics of the PPTh films before and after doping.

Table 6
Band gaps and other peaks from UV absorption

Energy (eV)	PTh [29–32]	PPTh(10)	PPTh(10,Ar)	PPTh(10,N_2)	PPTh(150)
E_g[a]	2–2.2	2.3	2.4	2.2	1.9
$(\pi-\pi^*)$[b]	2.6–3.0	2.8	2.8	–	–
Others[b]	1.2, 1.8	1.8	1.7, 2.1	1.4, 1.7	–

[a] From Mott plot.
[b] From Fig. 8.

as-deposited films are almost identical: non-linear, asymmetrical, and a maximum conductivity of 10^{-9} S cm^{-1} at the highest voltages. This non-linear behavior is typical of Schottky metal-semiconductor barriers with breakdown at reverse bias [33]. Schottky barriers exhibit an exponential relationship between current density (J) and voltage (V), as seen in Eqs. (4) and (5). The plot of ln J versus V should yield a straight line, if the Schottky barrier description is appropriate.

$$J = J_s \exp\left(\frac{qV}{nkT}\right) \tag{4}$$

$$J_s = AT^2 \exp\left(-\frac{q\phi_b}{kT}\right) \tag{5}$$

where J_s is expressed in Eq. (5), q is the charge on the charge carrier, k is Boltzman's constant, T is the temperature, n is the ideality factor (calculated from the slope of ln(J) versus V), A is the effective Richardson constant (the constant for silicon semiconductors, 120 A/(K^{2}cm^2), is often used for conjugated polymers) [28], and ϕ_b is the barrier height (calculated from the y-intercept of ln(J) versus V).

Ln(J) (forward bias) is plotted versus the absolute values of voltage for undoped PPTh(10,Ar) and undoped PPTh(150) in Fig. 11. Each data set has a significant data range that can be described by a straight line. The fit of the lines to the data is good, except at the lowest voltages. The barrier heights, taken from Fig. 11, lie between 0.8 and 0.9 eV (based on the Richardson constant for silicon) and are reasonable for the measured band gap. A typical value of n for metal-semiconductor barriers lies between 1 (thermo-ionic emission) and 2 (tunneling) [33]. Here, the n values, taken from Fig. 11, lie between 20 and 40, indicating that this is not a typical Schottky barrier. High values of n were also seen for conventional PTh [28]. PPTh(10,Ar) had a higher n value and a lower barrier height than PPTh(150).

Doping in iodine vapor produced a peak in the FTIR spectrum at 600 cm^{-1} and at 1170 cm^{-1} that were not seen in the undoped films (the $*$'s in Fig. 12). These peaks were associated with C–I groups [21]. Doping completely changed the IV characteristics of the films. Doped PPTh(150) developed ohmic IV characteristics, with the conductance significantly enhanced at low voltages (3.3×10^{-10} S cm^{-1}) (Fig. 10). Doped PPTh(10,Ar) exhibited ohmic behavior at high voltages in both forward and reverse (4.2×10^{-10} S cm^{-1}), but exhibited non-linear behavior at low voltages (Fig. 10). A conducting iodine percolation network seems to have formed in doped PPTh(150). Such a conducting iodine percolation network seems to form in doped PPTh(10,Ar) when ion mobility is enhanced at the higher voltages.

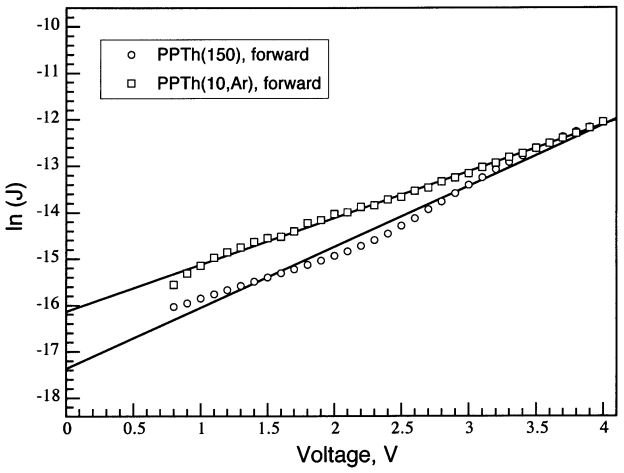

Fig. 11. Undoped films' IV characteristics (forward bias) fit to the Schottky model.

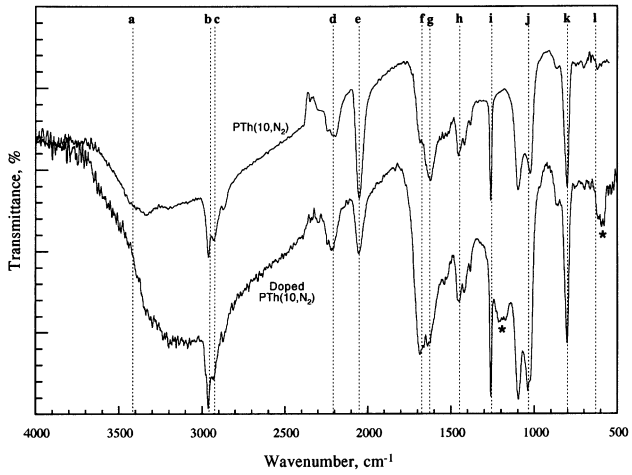

Fig. 12. FTIR spectra of PPTh(10,N_2) before and after doping.

4. Conclusions

Transparent plasma polymerized thiophene films, deposited at about 50 nm min^{-1}, had a density of about 1.75 g cc^{-1}, depending on the carrier gas used (if any) and on the plasma power. The molecular structure consisted of opened thiophene rings and included significant amounts of unsaturation, oxygen and nitrogen. The synthesis conditions affected the molecular structure and properties in the following manner:

- The carbon to sulfur ratio for the films at 10 W was about 6.3, as opposed to 4 in thiophene, reflecting the lower energy of the C–S bond compared to the C–C, C–O and C–N bonds. The lower C/S ratio for the film at 150 W was indicative of more intense fragmentation and etching and not indicative of a PTh-like structure.
- There was a significant increase in the amount of nitrogen and oxygen in the plasma polymer at 10 W when nitrogen was used as a carrier gas or at 150 W without a carrier gas. PPTh(10,N_2) and PPTh(150) include significant amounts of sulfur–oxygen bonds and ionized nitrogen while PPTh(10) and PPTh(10,Ar) do not.
- The E_g for the plasma polymerized thiophene films is about 2.2 eV, similar to that for conventional PTh. Several of the other electronic transitions seen in conventional PTh are also seen in plasma polymerized thiophene.
- The non-linear IV behavior of the undoped plasma polymerized thiophene films is typical of a Schottky metal-semiconductor barrier with breakdown at reverse bias. Doping in iodine vapor completely changed the IV behavior of the films. A conducting iodine percolation network seems to have formed in doped PPTh(150), yielding ohmic behavior. Such a conducting iodine percolation network seems to form in doped PPTh(10,Ar) when ion mobility is enhanced at the higher voltages.

Acknowledgements

The authors gratefully acknowledge the partial support of the Israeli Ministry of Science and of the Technion VPR Fund.

References

[1] Sethi RS, Goosey MT. In: Chilton JA, Goosey MT, editors. Special polymers for electronics and optoelectronics. London: Chapman & Hall, 1995. p. 1.
[2] Hotta S. In: Nalwa HS, editor. Handbook of organic conductive molecules and polymers, vol. 2. New York: Wiley, 1997. p. 309.
[3] Kaeriyama K. In: Nalwa HS, editor. Handbook of organic conductive molecules and polymers, vol. 2. New York: Wiley, 1997. p. 271.
[4] Samuelsen EJ, Mårdalen J. In: Nalwa HS, editor. Handbook of organic conductive molecules and polymers, vol. 3. New York: Wiley, 1997. p. 87.
[5] Yasuda H. Plasma polymerization. New York: Academic Press, 1985.
[6] Morosoff N. In: d'Agostino R, editor. Plasma deposition, treatment, and etching of polymers. New York: Academic Press, 1990. p. 1.
[7] Chen R, Gorelik V, Silverstein MS. J Appl Polym Sci 1995;56:615.
[8] Chen R, Silverstein MS. J Polym Sci Part A: Polym Chem 1996; 34:207.
[9] Silverstein MS, Chen R, Kesler O. Polym Eng Sci 1996;36:2542.
[10] Sandrin L, Silverstein MS, Sacher E. Polymer 2001;42:3761.
[11] Silverstein MS, Sandrin L, Sacher E. Polymer 2001;42:4299.
[12] Silverstein MS, Visoli I, Kesler O, Janai M, Cassuto Y. J Vac Sci Technol B 1998;16:2957.
[13] Zuri L, Silverstein MS, Narkis M. J Appl Polym Sci 1996;62:2147.
[14] Zuri L, Silverstein MS, Narkis M. Polym Eng Sci 1997;37:1188.
[15] Lee KP, Park SY, Kim N, Song SK. Mol Cryst Liq Cryst 1993; 224:53.
[16] Grünwald H, Munro HS, Wilhelm T. Mater Sci Eng A 1991;139: 356.
[17] Grünwald H, Munro HS, Wilhelm T. Synth Met 1991;41–43:1465.
[18] Bhuiyan AH, Bhoraskar SV. Thin Solid Films 1993;235:43.
[19] Sherwood PM. In: Briggs D, Seah MP, editors. Practical surface analysis by auger and X-ray photoelectron spectroscopy. New York: Wiley, 1983. p. 445.
[20] Tanaka K, Yoshizawa K, Takeuchi T, Yamabe T. Synth Met 1990; 38:107.
[21] Colthup NB, Daly LH, Wiberley SE. Introduction to infrared and Raman spectroscopy. 3rd ed. San Diego: Academic Press, 1990.
[22] Hummel DO. Atlas of polymer and plastic analysis. 3rd ed., vol. 1. Munich: VCH Publishers, 1991.
[23] Land TA, Hemminger JC. Surface Sci 1992;268:179.
[24] Streitwieser Jr. A, Clayton HH. Introduction to organic chemistry. New York: Macmillan, 1976.
[25] Beamson G, Briggs D. High resolution XPS of organic polymers. New York: Wiley, 1992.
[26] Moulder JF, Stickle WF, Sobol PE, Bomben KD. In: Chastain J, editor. Handbook of X-ray photoelectron spectroscopy. Eden Prairie: Perkin Elmer, 1992.
[27] Mott NF, Davis EA. Electronic processes in non-crystalline materials. 2nd ed. Oxford: Clarendon Press, 1979.
[28] Shin DH, Lee DS, Lee KP, Park SY, Choi DH, Kim N. Synth Met 1995;71:2263.
[29] Stockert D, Kessel R, Schultze JW. Synth Met 1991;41-43:1295.
[30] McKenzie RH, Wilkins JW. Synth Met 1991;41–43:3615.
[31] Hanawa T, Kuwabata S, Hashimoto H, Yoneyama H. Synth Met 1989;37:173.
[32] Pei Q, Inganas O, Osterholm JE, Laakso J. Polymer 1993;34:247.
[33] Bar-Lev A. Semiconductors and electronic devices. 2nd ed. New York: Prentice-Hall, 1984.